Supplementary Data

Characterization of Ada-G^{D}F^{D}F^{D}YG^{D}K-NH$_2$: ^{1}H NMR (300 MHz, DMSO-d_6) δ 9.15 (s, 1H), 8.15 – 7.98 (m, 4H), 7.89 – 7.82 (m, 2H), 7.33 (s, 1H), 7.17 (dd, *J* = 11.4, 4.7 Hz, 10H), 7.01 (d, *J* = 8.4 Hz, 2H), 6.62 (d, *J* = 8.4 Hz, 2H), 4.49 – 4.39 (m, 3H), 4.18 – 4.12 (m, 1H), 3.73 – 3.67 (m, 2H), 3.63 (d, *J* = 6.3 Hz, 1H), 3.51 (d, *J* = 5.3 Hz, 1H), 2.89 (d, *J* = 1.4 Hz, 2H), 1.87 (s, 2H), 1.84 (s, 3H), 1.60 (s, 2H), 1.54 (d, *J* = 8.7 Hz, 12H), 1.35 – 1.24 (m, 2H). MS: calc. M^+ = 892.4847, obsvd. $(M+H)^+$ = 893.4914, obsvd. $(M+Na)^+$ = 915.4720.

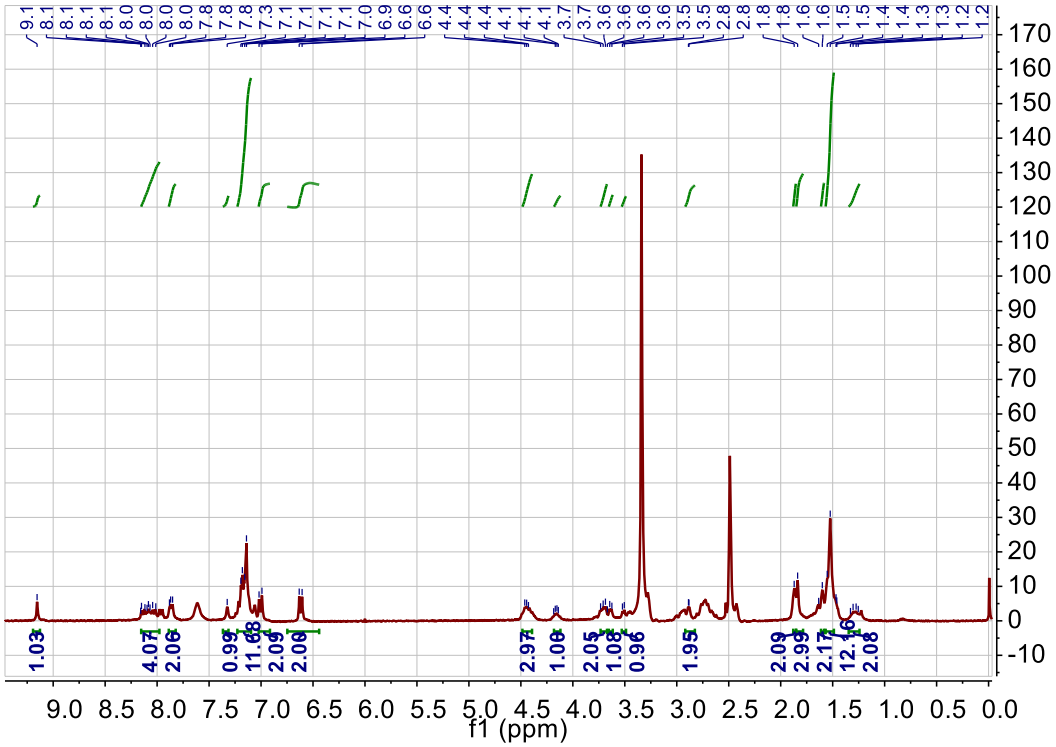

Figure S1. ^{1}H NMR spectrum of Ada-G^{D}F^{D}F^{D}YG^{D}K-NH$_2$.

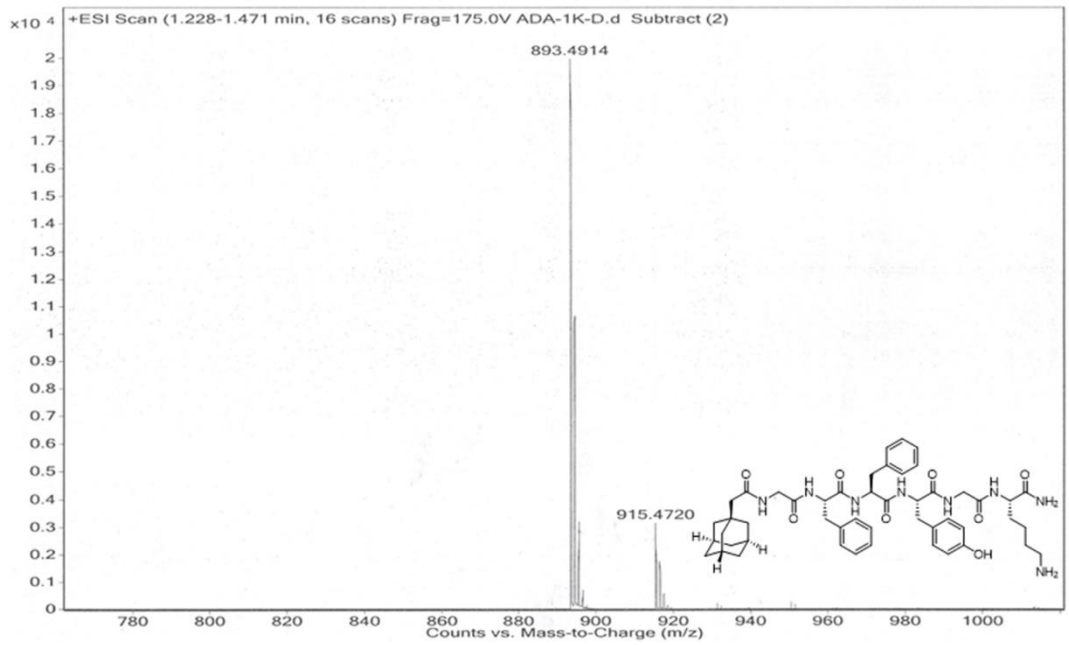

Figure S2. ESI-MS spectrum of Ada-G^{D}F^{D}F^{D}YG^{D}K-NH_2, insert was the corresponding chemical structure.

Characterization of Ada-G^{D}F^{D}F^{D}YG^{D}K^{D}K-NH_2: ^{1}H NMR (300 MHz, DMSO-d_6) δ 9.17 (s, 1H), 8.15 (d, *J* = 8.5 Hz, 1H), 8.06 (d, *J* = 3.8 Hz, 1H), 8.02 – 7.94 (m, 4H), 7.88 (t, *J* = 4.1 Hz, 1H), 7.29 (s, 1H), 7.23 (d, *J* = 6.2 Hz, 2H), 7.19 – 7.13 (m, 8H), 7.02 (s, 2H), 6.62 (d, *J* = 8.5 Hz, 2H), 4.53 – 4.37 (m, 4H), 4.29 – 4.23 (m, 1H), 4.13 (d, *J* = 8.1 Hz, 1H), 3.71 (d, *J* = 6.3 Hz, 2H), 3.64 (d, *J* = 7.1 Hz, 1H), 3.50 (s, 1H), 3.05 – 2.84 (m, 4H), 1.87 (s, 3H), 1.84 (s, 2H), 1.64 (s, 3H), 1.54 (d, *J* = 8.6 Hz, 16H), 1.34 – 1.25 (m, 4H). MS: calc. M^+ = 1020.5797, obsvd. $(M+H)^+$ = 1021.5850, obsvd. $(M+Na)^+$ = 1043.5688.

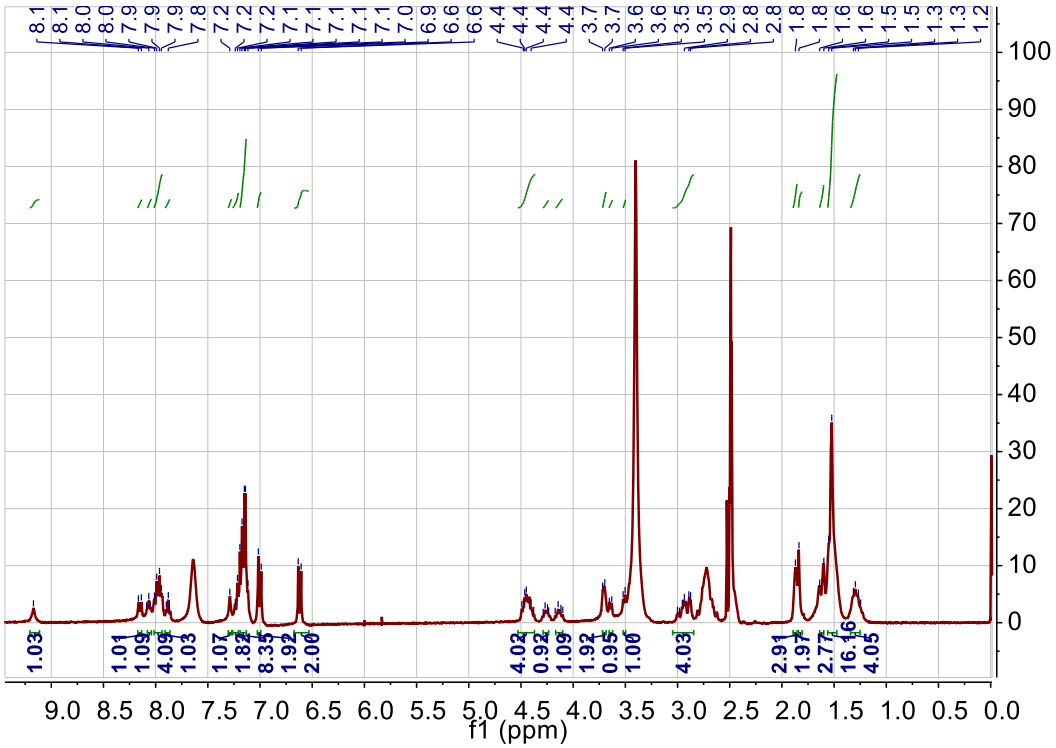

Figure S3. ^{1}H NMR spectrum of Ada-G^{D}F^{D}F^{D}YG^{D}K^{D}K-NH$_2$.

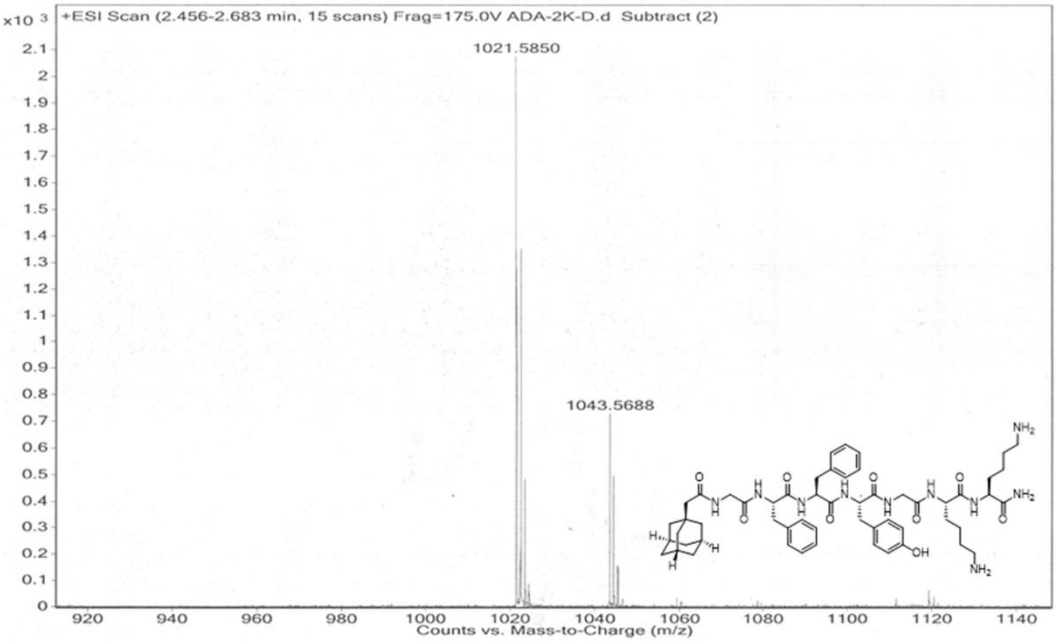

Figure S4. ESI-MS spectrum of Ada-G^{D}F^{D}F^{D}YG^{D}K^{D}K-NH$_2$, insert was the corresponding chemical structure.

Characterization of Ada-G^{D}F^{D}F^{D}YG^{D}K^{D}K^{D}K-NH$_2$: ^{1}H NMR (300 MHz, DMSO-d_6) δ 9.19 (s, 1H), 8.17 (s, 1H), 8.07 (s, 1H), 8.02 – 7.93 (m, 4H), 7.90 (d, J = 4.6 Hz, 1H),

7.82 (s, 1H), 7.35 (s, 1H), 7.21 (d, *J* = 6.9 Hz, 2H), 7.18 – 7.13 (m, 8H), 7.01 (d, *J* = 8.6 Hz, 2H), 6.63 (d, *J* = 8.4 Hz, 2H), 4.52 – 4.39 (m, 4H), 4.31 – 4.25 (m, 1H), 4.22 – 4.13 (m, 2H), 3.72 (d, *J* = 3.5 Hz, 2H), 3.66 (s, 1H), 3.03 – 2.88 (m, 4H), 1.86 (d, *J* = 9.7 Hz, 6H), 1.65 (s, 3H), 1.52 (t, *J* = 11.0 Hz, 22H), 1.36 – 1.26 (m, 6H). MS: calc. M^+ = 1148.6746, obsvd. $(M+H)^+$ = 1149.6773, obsvd. $(M+Na)^+$ = 1171.6614.

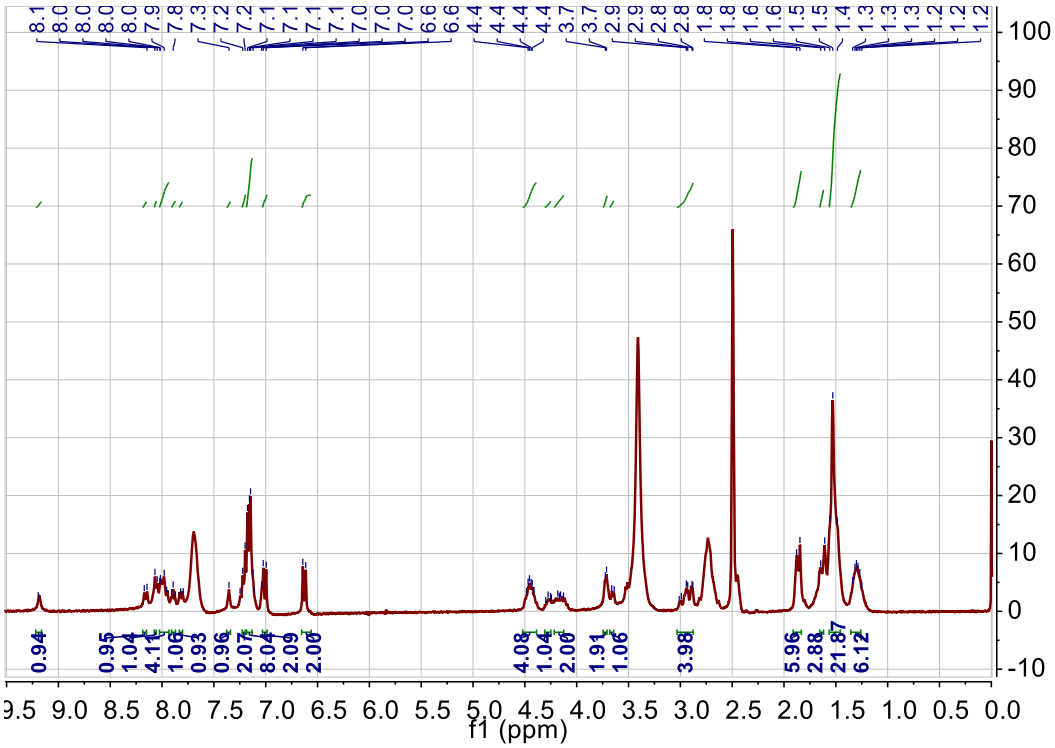

Figure S5. ^{1}H NMR spectrum of Ada-G^{D}F^{D}F^{D}YG^{D}K^{D}K^{D}K-NH_2.

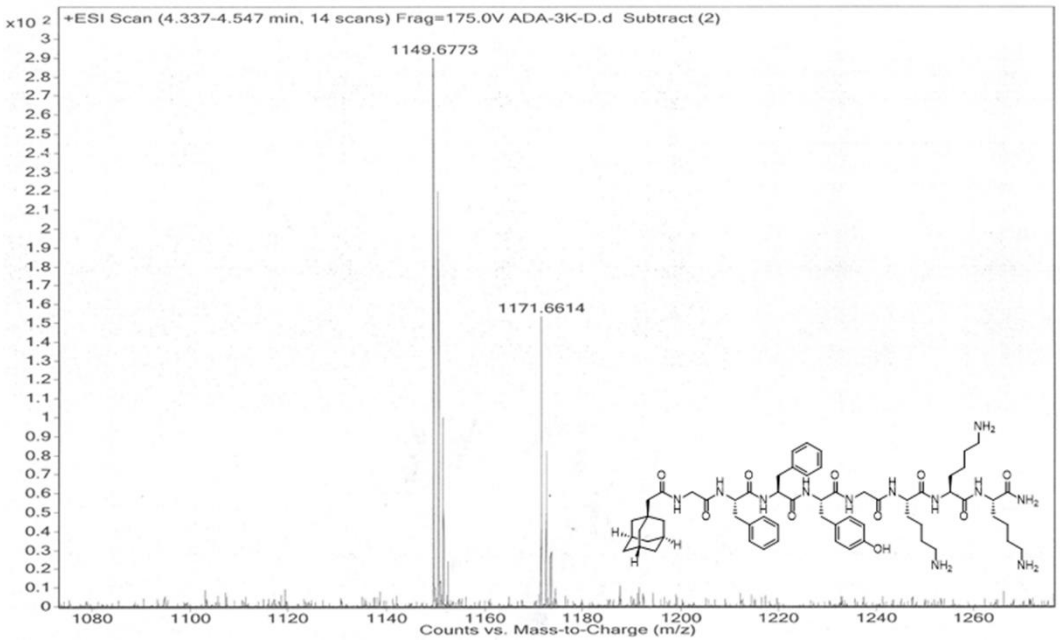

Figure S6. ESI-MS spectrum of Ada-G^{D}F^{D}F^{D}YG^{D}K^{D}K^{D}K-NH_2, insert was the corresponding chemical structure.

Characterization of Ada-GFFYGKKK-NH_2: ^{1}H NMR (300 MHz, DMSO-d_6) δ 9.19 (s, 1H), 8.18 (d, *J* = 8.4 Hz, 1H), 8.08 (d, *J* = 5.4 Hz, 2H), 8.05 – 7.96 (m, 4H), 7.89 (s, 1H), 7.36 (s, 1H), 7.20 (s, 2H), 7.16 (dd, *J* = 7.7, 2.8 Hz, 8H), 7.01 (d, *J* = 8.3 Hz, 2H), 6.63 (d, *J* = 8.4 Hz, 2H), 4.51 – 4.38 (m, 4H), 4.31 – 4.25 (m, 1H), 4.21 – 4.13 (m, 2H), 3.73 – 3.69 (m, 4H), 3.01 – 2.87 (m, 4H), 1.86 (d, *J* = 7.7 Hz, 6H), 1.66 (d, *J* = 6.8 Hz, 3H), 1.49 (s, 22H), 1.35 – 1.25 (m, 6H). MS: calc. M^+ = 1148.6746, obsvd. $(M+H)^+$ = 1149.6808, obsvd. $(M+Na)^+$ = 1171.6620.

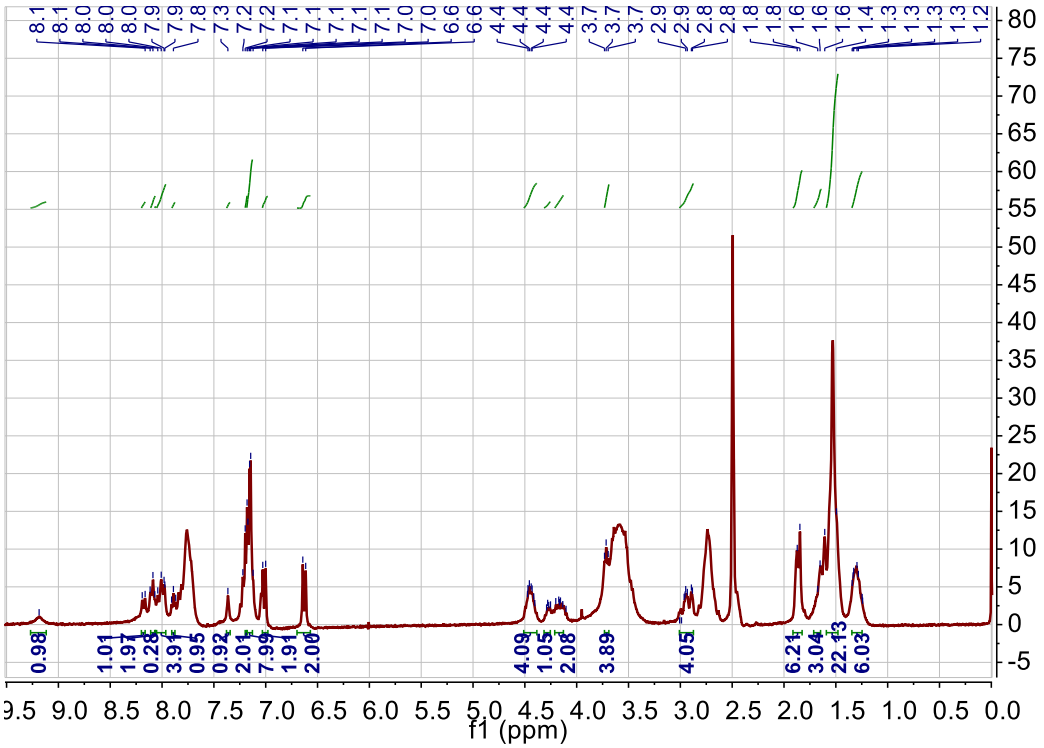

Figure S7. ^{1}H NMR spectrum of Ada-GFFYGKKK-NH_2.

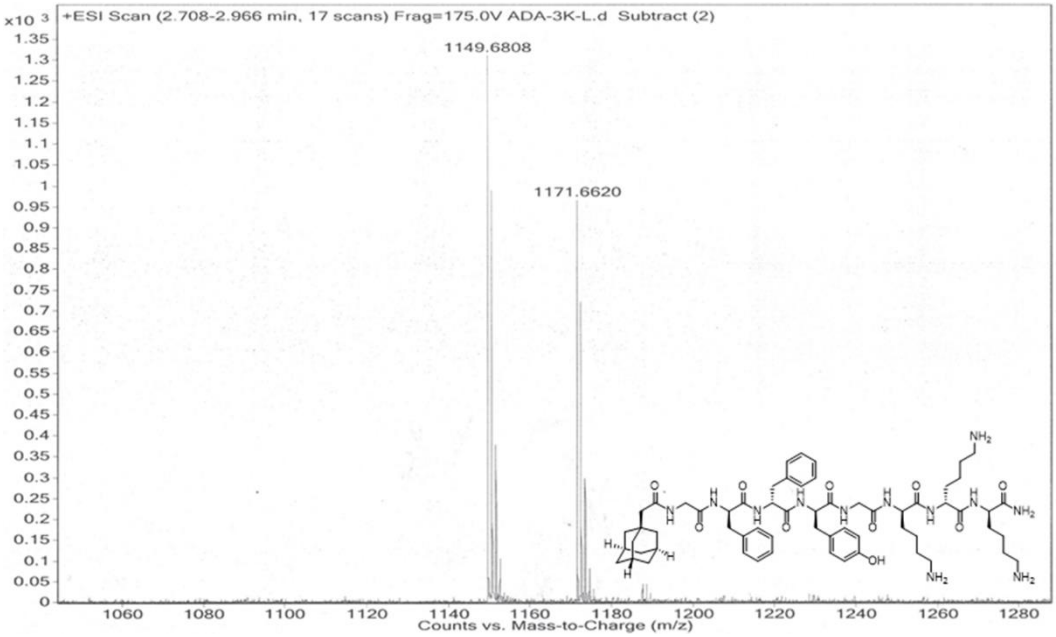

Figure S8. ESI-MS spectrum of Ada-GFFYGKKK-NH_2, insert was the corresponding chemical structure.

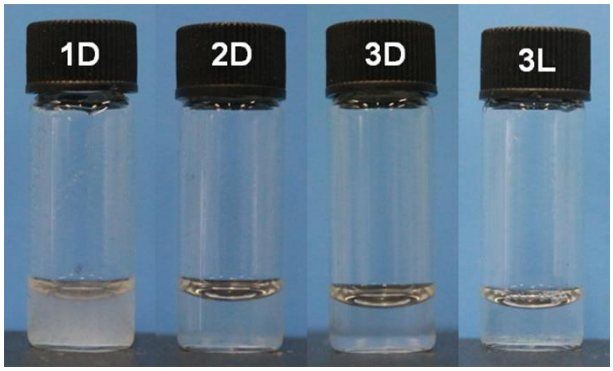

Figure S9. The optical picture of different peptide-derivates solution after adjusting pH value to 7.4 in PBS buffer.

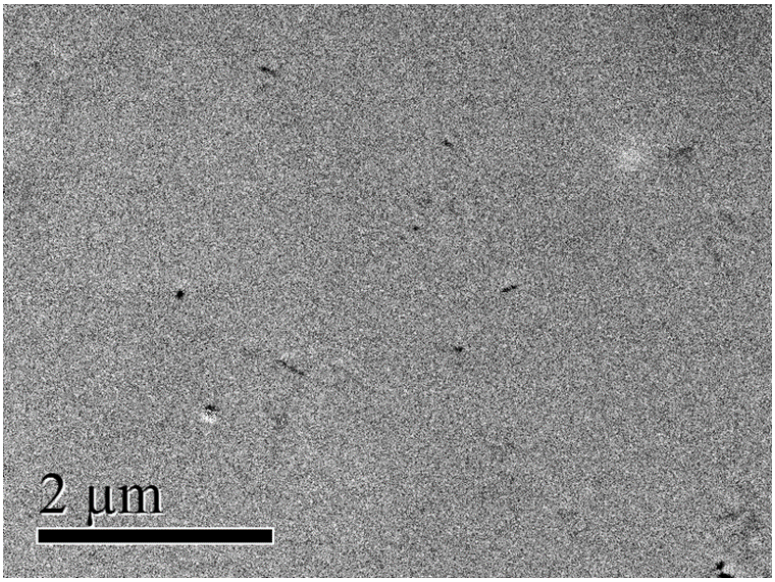

Figure S10. The TEM graph of 3DSNA at pH = 5.5 in PBS buffer.

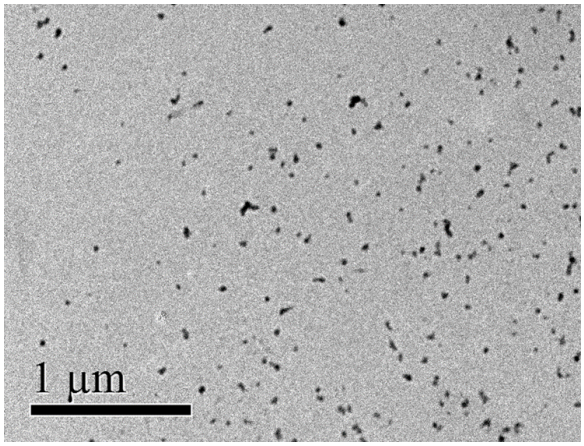

Figure S11. The corresponding TEM images of D-configurational peptide containing 4 K When the pH was adjusted to 7.4 in PBS buffer.

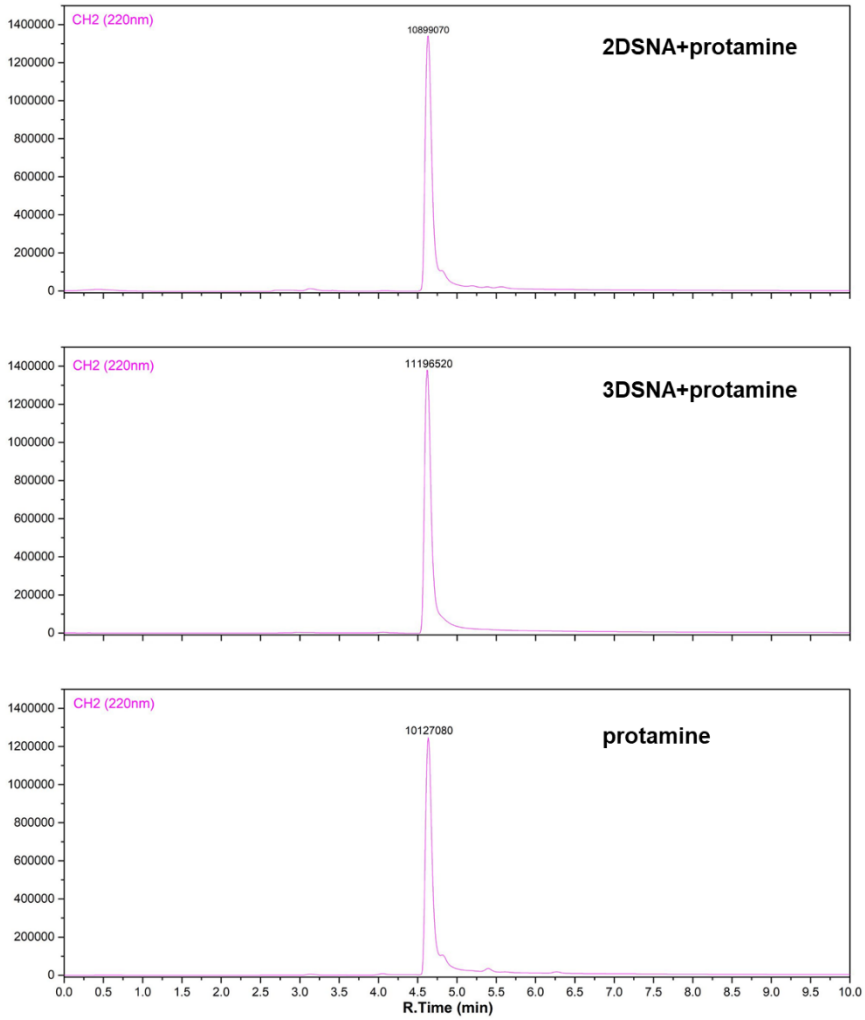

Figure S12. The HPLC analysis for the supernatant.

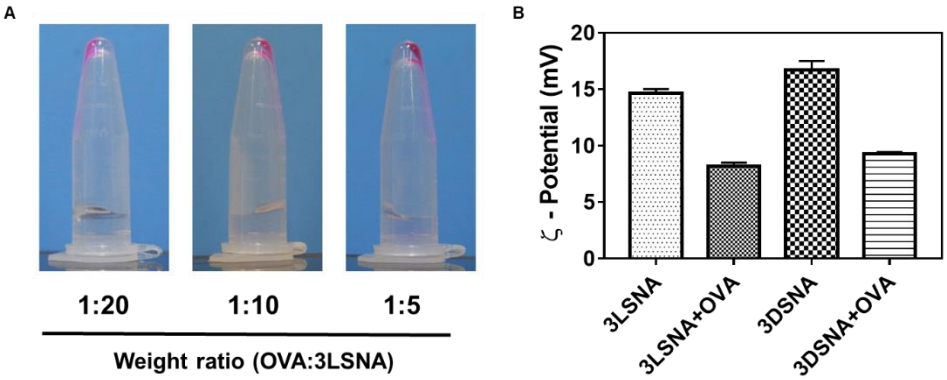

Figure S13. A) Optical picture of antigen absorbed by 3LSNA with different weight ratio. A) Zeta-potential of 3LSNA or 3DSNA and corresponding vaccine formulations

(OVA: 3LNSA or 3DSNA = 1:10).

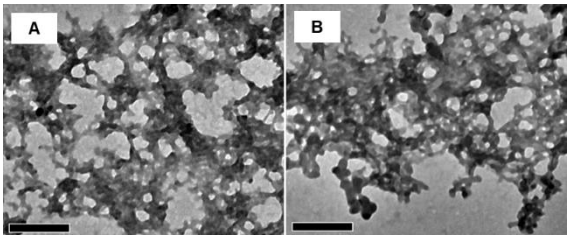

Figure S14. The TEM graph of A) 3DSNA+OVA and B) 3LSNA+OVA. Scale bar was 500 nm.

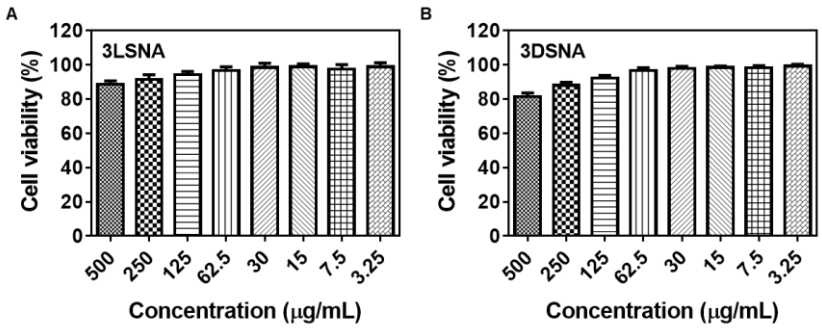

Figure S15. The biocompatibility of nanofiber-adjuvant.

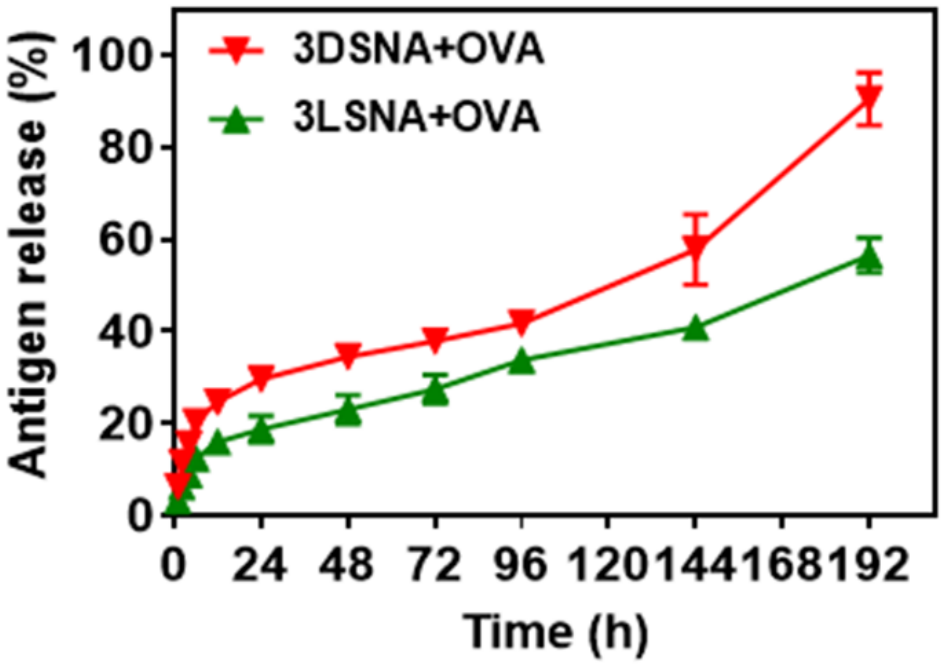

Figure S16. The release profiles of OVA from 3DSNA+OVA and 3LSNA+OVA.

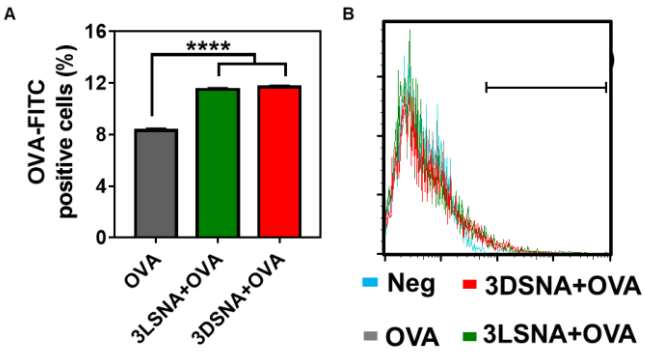

Figure S17. A) Percentage of BMDCs taking up FITC-OVA after incubation of free OVA, 3DSNA+OVA and 3LSNA+OVA for 1h measured by Flow cytometry. B) The corresponding histogram of BMDCs taking up FITC-OVA.

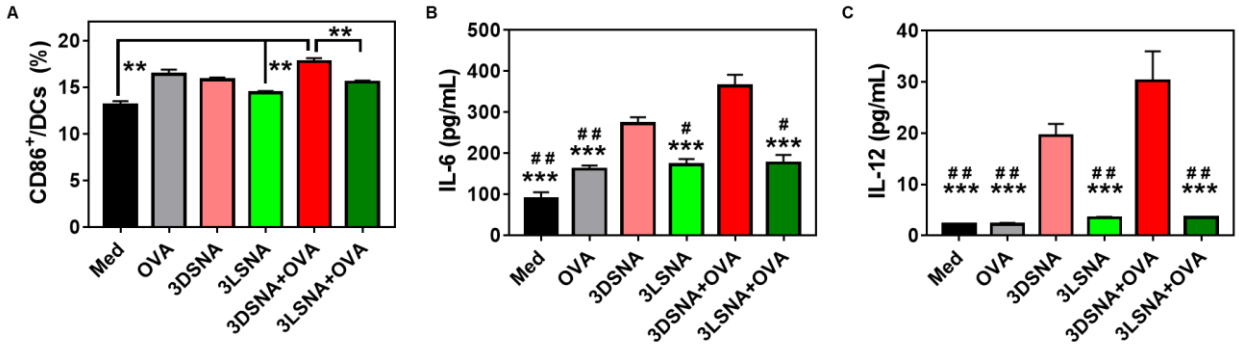

Figure S18. A) The percentage of CD86 expression (* $p < 0.05$, ** $p < 0.01$, n = 3), respectively, and production of B) IL-6 and C) IL-12 by BMDCs after incubation with different formulations for 24 h (*** $p < 0.001$, 3DSNA+OVA compared with others, # $p < 0.05$, # # $p < 0.01$, 3DSNA compared with others, n = 3). The data were analyzed by one-way ANOVA.

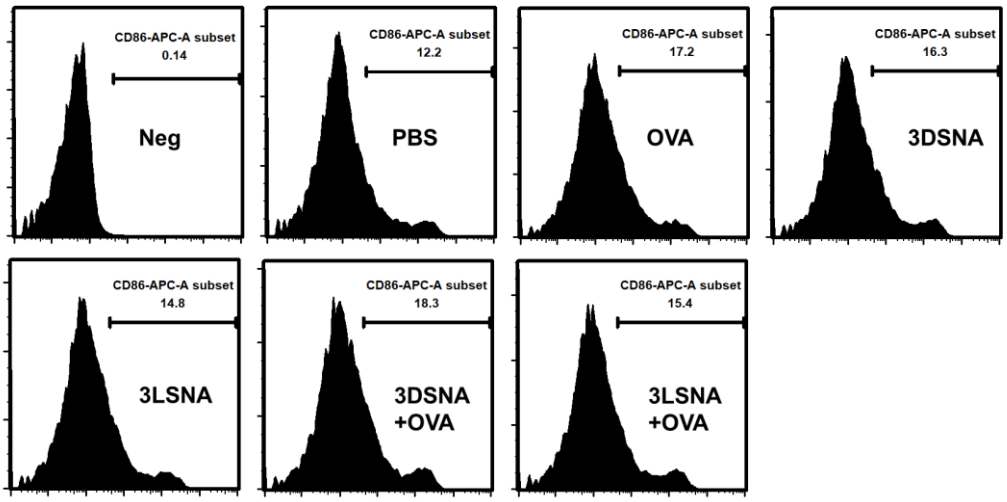

Figure S19. Histogram of CD86 of BMDCs treated by different vaccine formulations for 24 h.

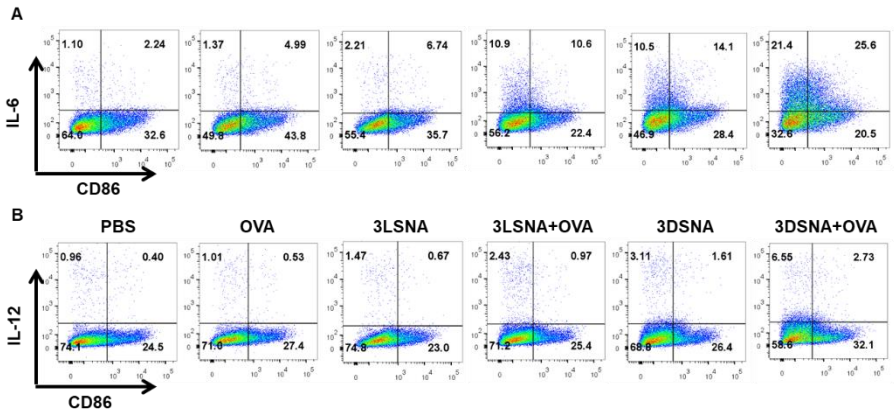

Figure S20. The representative dot pot for the A) $CD86^{+}$ $IL\text{-}6^{+}$ B) $CD86^{+}$ $IL\text{-}12^{+}$ among MCH Ⅱ + cells.

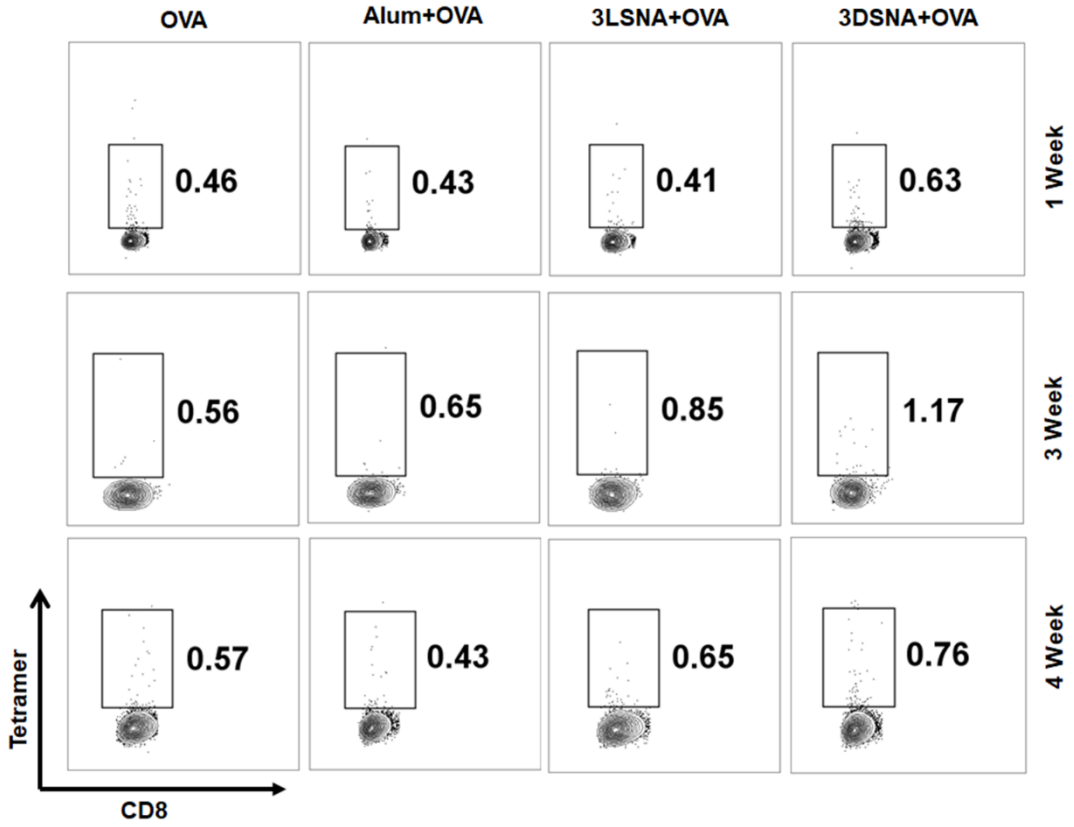

Figure S21. Frequency of SIINFEKL-specific T cells in peripheral blood assessed over time through flow-cytometry analysis of $tetramer^{+}$ $CD8^{+}$ T cells on 7, 21 and 28 day.

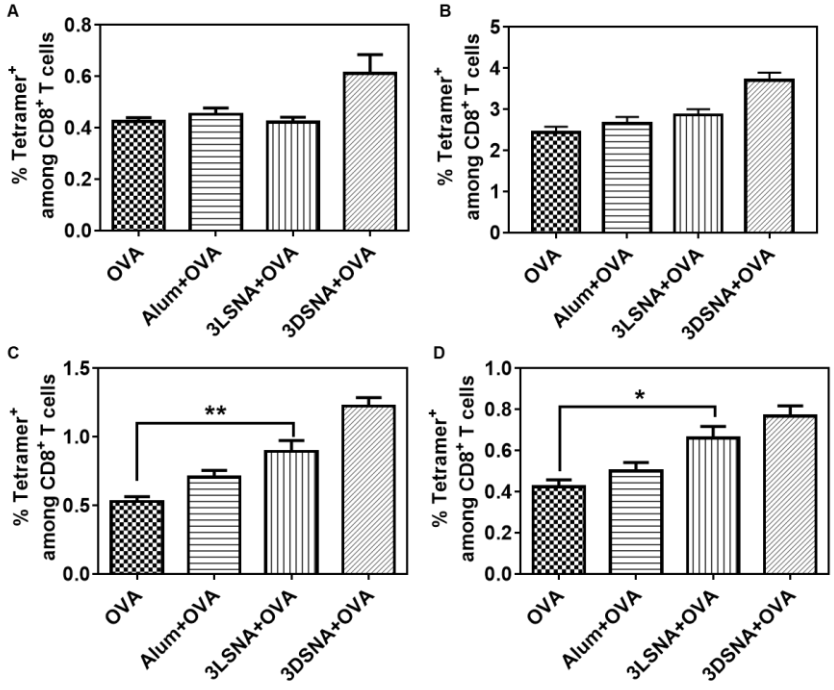

Figure S22. Percentage of SIINFEKL-specific T cells in peripheral blood assessed over time through flow-cytometry analysis of tetramer$^+$ CD8$^+$ T cells for vaccinations.

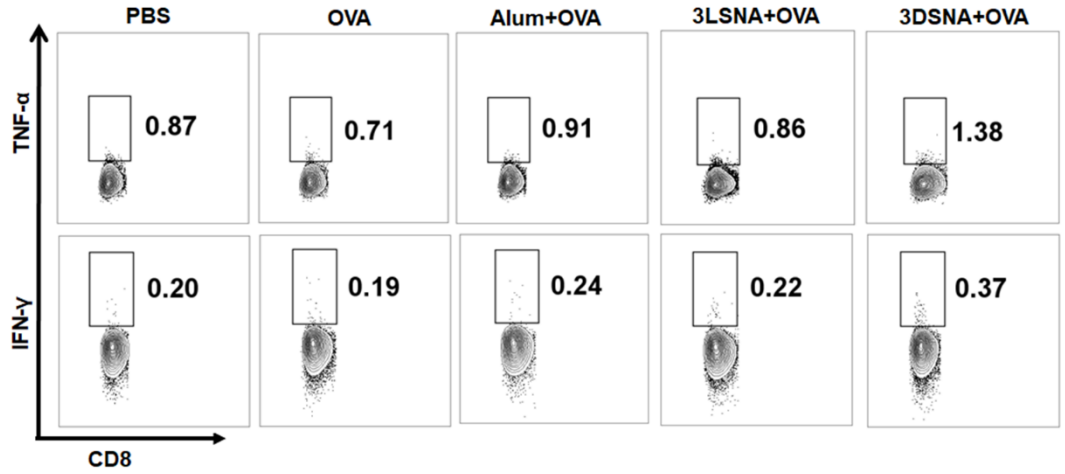

Figure S23. Flow cytometry dot plots for the frequency of IFN-γ^+ and TNF-α^+ among CD8$^+$ T cells in peripheral blood.